






Original Article

# Development and Characterization of Polycaprolactone Nanofibers Adorned with Gold Nanostars for Dental Bone Tissue Engineering

Alireza Koushki<sup>1</sup>, Sonia Fathi-Karkan<sup>2</sup>, Abolfazl Akbarzadah<sup>1</sup>, Parisa Besharati<sup>3</sup>, Saber Ganji<sup>4</sup>, Negar Sedghi Aminabad<sup>5</sup>, Shayesteh Fathi<sup>6</sup>, Maziar Malekzadeh Kebria<sup>6</sup>, Zahra Ebrahimvand Dibazar<sup>7\*</sup>, Seyedeh Parvaneh Moosavi<sup>8\*</sup>

<sup>1</sup>Department of Periodontics, Faculty of Dentistry, Hamadan University of Medical Sciences, Hamadan, Iran

<sup>2</sup>Department of Advanced Sciences and Technologies in Medicine, School of Medicine, North Khorasan University of Medical Sciences, Bojnurd, Iran

<sup>3</sup>Department of Orthodontics, Faculty of Dentistry, Shahed University of Medical Sciences, Tehran, Iran

<sup>4</sup>Department of Orthodontics, Faculty of Dentistry, Hamadan University of Medical Sciences, Hamadan, Iran

<sup>5</sup>Department of Medical Nanotechnology, Faculty of Advanced Medical Sciences, Tabriz University of Medical Sciences, Tabriz, Iran

<sup>6</sup>Department of Tissue Engineering and Regenerative Medicine, Faculty of Medicine, Hamadan University of Medical Sciences, Hamadan, Iran

<sup>7</sup>Department of Oral and Maxillo Facial Medicine, Faculty of Dentistry, Tabriz Azad University of Medical Sciences, Tabriz, Iran

<sup>8</sup>Department of endodontics, faculty of dentistry, Dental research center, Hamadan University of Medical Science, Hamadan, Iran

## Article history:

**Received:** March 15, 2025

**Revised:** April 28, 2025

**Accepted:** May 5, 2025

**ePublished:** Xx xx, 2025

## \*Corresponding authors:

Zahra Ebrahimvand Dibazar,

Email: [Dibazar20@gmail.com](mailto:Dibazar20@gmail.com);

Seyedeh Parvaneh Moosavi,

Email:

[parvanehmoosavi88@gmail.com](mailto:parvanehmoosavi88@gmail.com)

## Abstract

**Background:** Bone tissue engineering (BTE) provides an alternative to traditional treatments for severe bone defects that do not heal. Gold nanostructures enhance stem cell attachment to biocompatible scaffolds, thereby promoting their differentiation into osteoblasts. This study aimed to examine the use of electrospinning to create multilayered scaffolds that consist of polycaprolactone (PCL) and gold nanostars (GNSs).

**Methods:** This study developed a nanofiber-based scaffold composed of PCL and GNSs to improve bone tissue regeneration in adipose-derived stem cells (ADSCs) of rats while reducing the reliance on osteogenic differentiation media. GNSs were manufactured by the co-precipitation process and subsequently characterized using transmission electron microscopy (TEM) and dynamic light scattering (DLS). Next, a PCL-nanofibrous (NF) containing GNSs was created using the process of electrospinning. The resulting scaffold was then analyzed using scanning electron microscopy (SEM), energy-dispersive X-ray spectroscopy, contact angle measurements, tensile stretching tests, and Fourier-transform infrared spectroscopy (FTIR). ADSCs were subjected to treatment using PCL and PCL-GNS scaffolds for 1–3 weeks, both with and without the presence of osteogenic media conditions.

**Results:** An assessment was conducted to determine the vitality of the cells, their compatibility with blood, and their ability to differentiate into bone cells. The TEM and DLS results revealed that GNSs were produced as particles with a size range of 63 nm. The SEM scans demonstrated that the manufactured NF scaffolds were composed of nanofibers of 200–500 nm in size. FTIR spectroscopy investigation indicated that the natural structure of PCL and GNSs remained intact during the electrospinning process. Finally, GNSs enhanced the strength, wettability, porosity, and biocompatibility of the NF scaffold.

**Conclusion:** The findings confirmed that incorporating GNSs into the PCL matrix can enhance the osteogenic differentiation of stem cells, suggesting its potential application in BTE. This phenomenon has the potential to be applied in living organisms to facilitate the mending of bone defects. The results of this study suggest that combining PCL with GNSs can enhance the effectiveness of composite scaffolds in BTE therapies.

**Keywords:** Nanofiber, Polycaprolactone, Gold nanostar, ADSCs, Differentiation



**Please cite this article as follows:** Koushki A, Fathi-Karkan S, Akbarzadah A, Besharati P, Ganji S, Sedghi Aminabad N, et al. Development and characterization of polycaprolactone nanofibers adorned with gold nanostars for dental bone tissue engineering. *Avicenna J Dent Res.* 2025;17(3):x-x. doi:10.34172/ajdr.2338



© 2025 The Author(s); Published by Hamadan University of Medical Sciences. This is an open-access article distributed under the terms of the Creative Commons Attribution License (<https://creativecommons.org/licenses/by/4.0>), which permits unrestricted use, distribution, and reproduction in any medium, provided the original work is properly cited.

## Background

Bone abnormalities resulting from trauma or disease pose a significant clinical obstacle for global public health. The shortcomings of bone grafts have motivated researchers to investigate the field of bone tissue regeneration, restoration, and engineering (1,2). Overall, bone tissue engineering (BTE) has been developed to imitate autologous bone transplants by using living cells, scaffolds, and growth factors (3). Adipose-derived stem cells (ADSCs) are versatile cells capable of differentiating into various specialized cell types, such as chondrocytes, osteoblasts, myoblasts, and neural cells. ADSCs have demonstrated a notable affinity for scaffold material and a strong ability to transform into osteogenic cells. ADSCs release growth factors that have a role in the process of bone tissue remodeling and the formation of new blood vessels (angiogenesis). ADSCs, in comparison to bone marrow-derived mesenchymal stem cells, can be acquired in a high proportion, are readily accessible and collectible, and have a reduced susceptibility to senescence (4). Typically, osteogenic media contain cytokines and growth factors for BTE. Nevertheless, these media come at a high cost, and any alterations in their composition can impact the differentiation of ADSCs into non-targeted cells. Furthermore, media growth factors have a brief period of effectiveness, leading to a quick decline in their actions within a living organism (5). Therefore, there is a need to create a cost-efficient and customized framework that requires the least amount of osteo media. The scaffold is essential in the development of artificial bone. The objective is to replicate the physiochemical characteristics of the native tissue extracellular matrix (ECM) and facilitate cell attachment, proliferation, and osteogenic differentiation (6). Polycaprolactone (PCL) is a polymer that has been recognized by the United States Food and Drug Administration. It possesses favorable biocompatibility, thermal stability, and hydrophobic properties, enabling it to promote the adherence of stem cells. As a result, PCL is well-suited for use in BTE. The gradual breakdown of PCL poses difficulties in the field of soft tissue engineering but renders it a suitable substance for hard tissues like bone (7). The electrospun PCL scaffold, characterized by its high porosity, promotes cell proliferation, rearrangement, and nutrient exchange. Nevertheless, a high level of porosity diminishes the mechanical strength of PCL. This can be enhanced by regulating the ratio of pores and employing a specific technique for constructing a multilayered three-dimensional structure (8). Recent research has found that applying a layer of gold nanostars (GNSs) to the surface of a polymeric scaffold can enhance cellular adherence and provide differentiation stimuli at the nanoscale (9). GNSs enhance the roughness and surface area, hence increasing the number of sites for stem cell adhesion. Additionally, GNSs bring osteoconductive and osteoinductive effects, which expedite the healing of bone defects (10,11). Nevertheless, they impair ADSC's capacity to undergo adipogenic differentiation (12). The presence of gold

nanoparticles (GNPs) in a rat model increases the activity of alkaline phosphatase and the amount of calcium, suggesting that GNPs can stimulate the formation of new bone tissue (osteogenesis) and the growth of new blood vessels (angiogenesis) (13). GNPs also stimulate the mitogen-activated protein kinase signaling pathways to enhance the process of osteogenic differentiation in bone marrow-derived mesenchymal stem cells (14). In comparison to PCL scaffolds, the incorporation of GNPs into PCL scaffolds results in a tissue-biocompatible scaffold that promotes cell adhesion, proliferation, and mineralization. In addition, it stimulates the growth of new blood vessels, facilitating the process of bone repair and regeneration in living organisms (15). Furthermore, the incorporation of GNPs into PCL allows for self-reinforcement, resulting in improved strength. The GNSs can be loaded into the scaffold using electrospinning and layer-by-layer (LbL) techniques. Electrospinning offers a significant ratio of surface area to volume, the capacity to adjust fiber diameters, a high level of porosity, and permeability (16). The process of LbL assembly creates multilayer films composed of a scaffold material, which enhances the adhesion and proliferation of stem cells. Furthermore, the utilization of electrospinning and LbL assembly not only improves the structural integrity of GNS scaffolds but also stimulates the process of osteogenic differentiation in ADSCs (17). Overall, the enlarged scaffolds have the potential to be a valuable ECM in the field of BTE. This study seeks to investigate the use of electrospinning in order to create multilayered scaffolds consisting of PCL and GNSs. It has been hypothesized that the artificially created scaffold can improve the adhesion of ADSCs and boost the osteogenic effect through synergy. To test our idea, many cellular, molecular, and experimental experiments have been conducted in a controlled laboratory setting. This technology has the potential to enhance the design of future scaffolds with inherent stimuli from GNSs for BTE.

## Materials and Methods

### Materials

Hydrogen tetrachloroaurate ( $\text{HAuCl}_4$ ,  $\geq 99.9\%$ ), 3-(4,5-dimethylthiazol-2-yl)-2,5-diphenyltetrazolium bromide (MTT), polyvinylpyrrolidone ( $M_w = 40000$  g/mol), dimethyl sulfoxide (DMSO), and dimethyl formamide were purchased from Sigma-Aldrich Company. Sodium citrate ( $> 99\%$ ), silver nitrate, ascorbic acid, hydrochloric acid, sodium chloride, sodium bromide, and sodium sulfide (55%) were obtained from Merck Company. Deionized water with a resistance greater than  $18.2 \text{ M}\Omega$  was utilized in all experiments. Additional materials, including penicillin-streptomycin, fetal bovine serum, trypsin, and Roswell Park Memorial Institute medium, were purchased from Gibco BRL Life Technologies. Eventually, PCL with a molecular weight of  $150,000 \text{ Da}$  was obtained from Alfa Chemistry (NY, USA).

### Preparation of Gold Nanostars

GNSs were manufactured utilizing a previously described two-step approach called seed-mediated growth (18). They were produced using the Turkevich process, with an estimated size of 13 nm. The surfactant-free approach was employed to perform the procedure (19). GNP seeds were generated by reducing  $\text{HAuCl}_4$  (100 mL, 1 mM) with trisodium citrate (15 mL, 1% w/v). The GNS was synthesized by the rapid and simultaneous addition of silver nitrate (1 mL, 3 mM) and ascorbic acid (500  $\mu\text{L}$ , 0.1 M) to a solution containing 0.25 mM  $\text{HAuCl}_4$ , 1 mM hydrochloric acid, and 1 mL of GNP seeds prepared in the previous step.

### Nanostructure Characterization

The optical properties of the produced GNPs and GNSs were examined using a UV-Vis spectrophotometer manufactured by SHIMADZU. Transmission electron microscopy (TEM) imaging was conducted using a LEO 906 TEM (manufactured in Germany by Zeiss). These analyses were performed to investigate the particle size and morphology of GNPs and GNSs. Dynamic light scattering (DLS) and zeta potential ( $\zeta$ ) measurements were conducted using Malvern Instruments (Malvern, UK) to determine the hydrodynamic size and surface charge of GNPs and GNSs. Additionally, ICP-OES (Perkin-Elmer, Waltham, MA, USA) was employed to quantify the gold ion concentration.

### Preparation of Gold Nanostar-Adorned Polycaprolactone Nanofiber

Nanofibers composed of PCL and GNSs were fabricated by utilizing a simple one-step procedure. The technique of electrospinning was adopted to produce PCL nanofibers, which served as a scaffold for GNSs and facilitated the flow of fluids as a filtration membrane. First, PCL nanofibers were deposited onto aluminum foils using the electrospinning technique. PCL (10% v/w) and GNSs (80 ppm/mL) were dissolved in a *dimethylformamide* solution and administered using a syringe pump at a flow rate of 0.5 mL/h.

### Characterization of Fabricated Scaffolds

#### Scanning Electron Microscopy, Energy Dispersive X-Ray Spectroscopy, and Contact Angle

Prior to microscopic investigations, the samples were coated with a thin layer of gold using a sputter-coating technique in order to enhance surface conductivity and prevent surface charge. The NFs were analyzed using a scanning electron microscope with EDS to examine their morphology and semi-quantitative elemental characteristics. The scaffolds were also examined using a static contact angle measurement instrument (KRÜSS, Hamburg, Germany) to determine the water contact angles of deionized water on three portions of each scaffold, which were then averaged.

### Fourier-Transform Infrared Spectroscopy

Functional groups present in the fabricated scaffolds were identified using FTIR spectroscopy. To this end, the dried scaffold samples were sectioned into discs measuring 10 mm in diameter and 1 mm in thickness. The analysis was performed over a wavenumber range of 600–4000  $\text{cm}^{-1}$ .

### Porosity

The porosity of the synthesized NF was evaluated by analyzing SEM images using the ImageJ software. Porosity was determined by dividing the total surface area of the pores by the overall area of each image. This analysis was performed on a series of SEM images, and the average values were reported. Additionally, the pore size and the pore size distribution were calculated by randomly measuring the dimensions of at least 100 pores across multiple SEM images.

### Mechanical Testing

The compressive mechanical properties of the scaffolds were evaluated through monotonic uniaxial unconfined compression testing, following a previously established methodology (20). Cylindrical scaffolds were prepared for each composition, with at least three replicates per group. To simulate physiological conditions, the samples were immersed in phosphate-buffered saline (PBS) for one hour before testing. Mechanical testing was performed at room temperature using a universal mechanical tester at a crosshead speed of 1 mm/min. The elastic modulus of each scaffold was determined from the slope of the linear portion of the stress-strain curves obtained during testing.

### Swelling Behavior

The swelling characteristics of the constructed scaffolds were assessed using a methodology outlined elsewhere (21). The initial mass of each scaffold, with a diameter of 10 mm and a thickness of 5 mm, was measured. The scaffold was then placed in a solution of PBS and incubated in a controlled environment at a temperature of 37 °C. Subsequently, the samples were weighed at specific time intervals after eliminating any surplus water from the scaffolds' surface. The swelling ratio of the scaffolds was determined according to the following equation:

$$\text{Swelling ratio} = (\text{Ww} - \text{Wd}/\text{Wd}) \times 100$$

Where Ww denotes the weight of the wet sample, while Wd refers to the initial dry weight of the same sample. The results are presented as means  $\pm$  standard deviations (SD), calculated from measurements obtained from three independent samples.

### In Vitro Degradation Study

The in vitro degradation assay was conducted using the methodology described in previous research (21). Prior to the in vitro hydrolytic degradation experiments, the samples were immersed in PBS for 2 hours to achieve

swelling equilibrium, after which they were weighed. This measurement was considered the initial weight (time zero). Subsequently, the scaffolds were incubated in PBS for a period of 21 days to evaluate their degradation behavior. At specified time intervals, the samples were extracted from PBS, and the weight of each sample was determined. The degradation percentage was measured as follows:

$$\text{Degradation (\%)} = (W_t - W_i / W_i) \times 100$$

$W_i$  and  $W_t$  represent the starting weight of the sample and the weight of the sample at different time intervals, respectively. The mean  $\pm$  SD values were calculated from data collected from three scaffolds.

### Hemolysis Induction Assay

The artificial NF-based scaffolds (50 mg) were exposed to 200  $\mu$ L of recently collected and anticoagulated blood (diluted with PBS, 2:2.5) at 37 °C for 1 hour. Next, the samples underwent centrifugation at a speed of 1,500 revolutions per minute for 3 minutes at 40 °C. Ultimately, the intensity of light absorbed by the liquid remaining after centrifugation was measured at a wavelength of 545 nm using a device designed for analyzing samples in microplates. The following equation was applied to calculate the hemolysis percentage:

$$\text{Hemolysis (\%)} = (D_t - D_{nc} / D_{pc} - D_{nc}) \times 100$$

Where  $D_t$ ,  $D_{nc}$ , and  $D_{pc}$  denote the absorbance values of the sample, negative control, and positive control, respectively.

### Cell Toxicity Analysis

The biocompatibility of the synthesized GNSs and fabricated scaffolds was assessed via in vitro cytotoxicity testing using the MTT assay. ADSCs were cultured in the Dulbecco's modified Eagle's medium with 10% fetal bovine serum and 1% penicillin/streptomycin. GNS powders were uniformly dispersed in the culture medium at various concentrations, sterilized by filtration, and incubated with the cells for 24 hours at 37 °C prior to assessing cell viability. ADSCs were placed into 96-well plates with a density of  $3 \times 10^3$  per well. After the cells were attached, the particle suspensions were added to refresh the culture media, and this moment was designated as the start of the culture time. At predetermined intervals (1 day, 2 days, and 3 days), the scaffolds were assessed for cell activity using the MTT assay. The MTT solution (0.5 mg/mL) was added to each well and incubated at 37 °C for 4 hours. After incubation, the medium was discarded, and 100  $\mu$ L of DMSO was added to dissolve formazan crystals, followed by 15 minutes of agitation in the dark. The absorbance at 570 nm was measured using a microplate spectrophotometer. The scaffolds, sectioned into 1 mm-thick discs (6 mm in diameter, ~2.4 mg

each), were sterilized by immersion in 70% ethanol and exposure to UV light for 2 hours. They were then rinsed with PBS and culture medium before being seeded with ADSCs ( $5 \times 10^4$  cells per scaffold) in a 48-well plate. The culture medium was refreshed every other day. At 3-day, 5-day, and 7-day intervals, the MTT solution was added, incubated, and dissolved with 150  $\mu$ L of DMSO, followed by agitation in the dark for 15 minutes. Absorbance at 570 nm was recorded using a microplate spectrophotometer after transferring the solution to a 96-well plate.

### Statistical Analysis

All quantitative data are presented as means  $\pm$  SDs. Statistical analyses were conducted using GraphPad. One-way analysis of variance was performed, followed by Tukey's post hoc test to determine significant differences between groups. A  $P$  value of less than 0.05 was considered statistically significant for all comparisons.

## Results and Discussion

### Characterization of Gold Nanostars

GNSs were synthesized using galvanic replacement techniques. TEM imaging was utilized to determine the average sizes of both GNPs (obtained via a seed-mediated approach) and the resulting GNSs (Figure 1). Based on localized surface plasmon resonance spectroscopy, the wavelength at which the greatest absorption peaks occurred was 648 nm (Figure 1A). The TEM pictures revealed that the synthesized GNSs possess a uniform star-like morphology with a diameter of around 63 nm

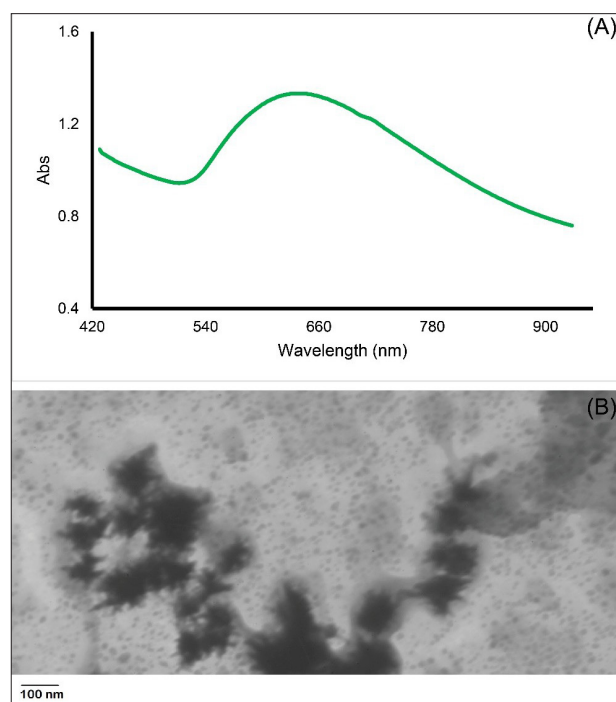


**Figure 1.** TEM Images and UV-Vis Spectroscopy Employed to Characterize the Synthesized GNSs: (A) TEM Analysis and (B) The UV-Vis Absorption Spectra of GNSs. Note: TEM: Transmission electron microscopy; GNS: Gold nanostar. (A) The analysis revealed that the GNSs have an average size of  $63.2 \pm 8.2$  nm. (B) The spectra exhibited a maximum absorption peak at 648 nm



(Figure 1B). The TEM data further demonstrated that the sample has a limited distribution of particle sizes. The DLS analysis represented an average size of around 273 nm, accompanied by a tightly concentrated nanoparticle size distribution (Figure 2). The nanoparticle size detected using transmission TEM is less than the hydrodynamic diameter estimated using DLS. The literature often reports variations in DLS and TEM results. This is because DLS measures the hydrodynamic size, which implies that the recorded particle size is generally greater than the actual particle size. In addition, the seldom occurrence of sizable particles, along with the formation of fragile particle clusters, can lead to a rise in the z-average particle size (22).

### Characterization of the Fabricated Nanofiber-Based Scaffolds

SEM images revealed the porous architecture of the four different scaffold types, highlighting a rough surface morphology conducive to stem cell attachment and facilitating the development of cells with specific morphologies. EDS mapping and profiles confirmed the incorporation of GNSs within the scaffolds, as indicated by the presence of the Au element (Figure 3). The FTIR spectra of PCL and PCL-GNS scaffolds are presented in

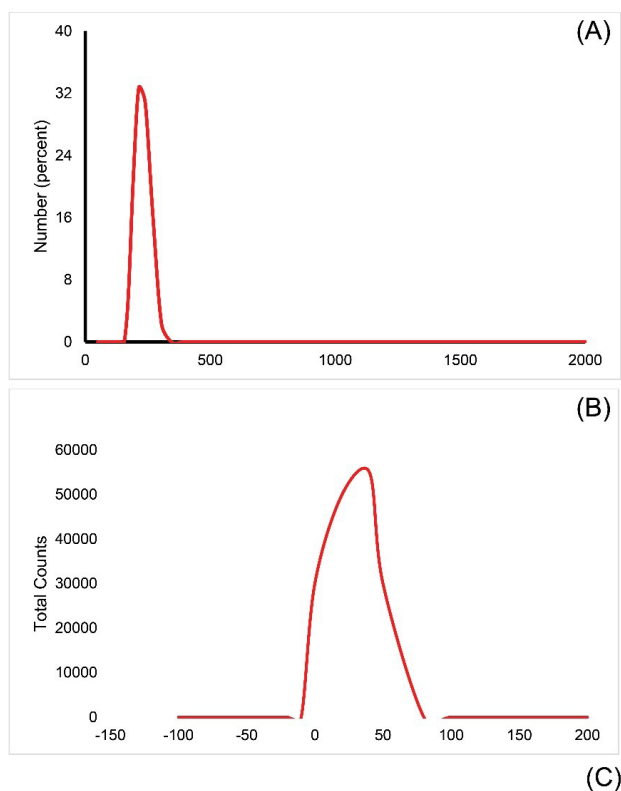


**Figure 2.** The Size Distribution and Zeta Potential of the Synthesized GNSs: (A) Size Distribution Histogram Illustrating the Range and Frequency of GNS Size, (B) Zeta Potential Measurement Indicating the Surface Charge and Stability of GNSs in Suspension, and (C) Hydrodynamic Diameter, PDI, and Zeta Potential Values for GNSs, Providing Comprehensive Characterization of Their Colloidal Properties. *Note.* GNS: Gold nanostar; PDI: Polydispersity index

Figure 4A. Characteristic absorption bands observed at  $1424\text{ cm}^{-1}$  and  $1070\text{ cm}^{-1}$  correspond to the stretching vibrations of  $-\text{COOH}$  groups and  $\text{C}-\text{O}$  groups, respectively. Additionally,  $\text{C}=\text{O}$  groups in the scaffolds were detected at  $1608\text{ cm}^{-1}$ ,  $1617\text{ cm}^{-1}$ , and  $1624\text{ cm}^{-1}$ . The signal detected at  $1088\text{ cm}^{-1}$  matches the vibrations of  $\text{C}-\text{C}$ , providing evidence of the existence of GNSs in PCL scaffolds. The surface wettability of electrospun nanofibrous (NF) materials plays a critical role in their application for tissue engineering. In this study, water contact angle (WCA) measurements were conducted to evaluate the wettability of the scaffold surfaces. According to the literature, materials exhibiting WCA values between  $40^\circ$  and  $70^\circ$  are classified as moderately hydrophilic, which is considered optimal for promoting cell adhesion, spreading, and proliferation. In contrast, highly hydrophilic ( $\text{WCA} < 20^\circ$ ) or hydrophobic ( $\text{WCA} > 90^\circ$ ) surfaces are generally less favorable for these cellular processes (23). Appropriate bone tissue should have hydrophilic properties. The hydrophilicity of the produced scaffold was assessed by measuring the water contact angles. The findings indicate that the inclusion of GNSs into PCL nanofibers leads to a reduction in water contact angles (Figures 4C, 4D, and 4E). The porosity of the constructed PCL and PCL@GNSs was determined to be  $73.4\% (\pm 2.5\%)$  and  $83.1\% (\pm 1.6\%)$ , respectively (Figure 4F). The constructed scaffolds had a range of pore sizes, varying from less than  $5\text{ }\mu\text{m}$  to  $60\text{ }\mu\text{m}$ . The mean pore diameter of the PCL and PCL@GNSs scaffolds was  $22.1\text{ }\mu\text{m}$  and  $25.6\text{ }\mu\text{m}$ , respectively.

### Mechanical Testing

The mechanical stability of the scaffolds was assessed by evaluating their resistance to vertical change and estimating the elastic modulus. The mechanical durability of the scaffolds was assessed by immersing them in a PBS solution to mimic physiological circumstances (Figure 4B). The mechanical strength of our produced

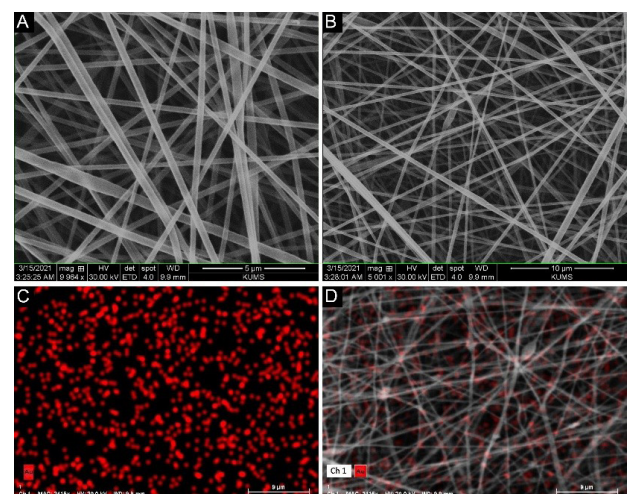


**Figure 3.** SEM Images of the Fabricated NF: (A) PCL-NF, (B) PCL-GNS-NFs, and (C, D) Corresponding EDS Analyses of the Fabricated NF. *Note.* SEM: Scanning electron microscopy; PCL: Polycaprolactone; GNS: Gold nanostar; NF: Nanofibrous; EMS: Energy-dispersive X-ray spectroscopy

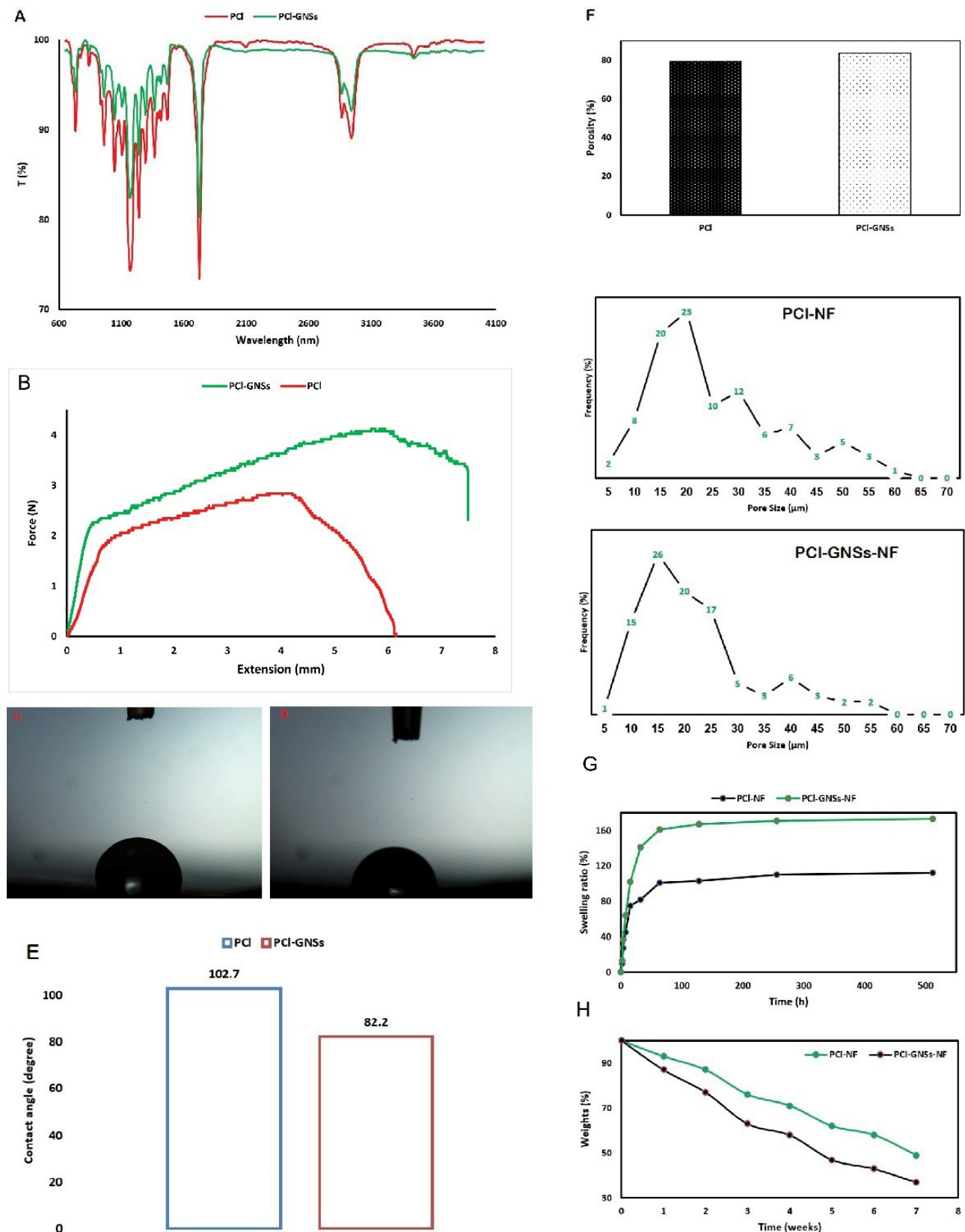


**Figure 4.** (A) FTIR Spectra of PCI and PCI@GNS Nanofiber-Based Scaffolds, (B) Mechanical Properties of Fabricated Scaffolds, (C–E) Surface Wettability Analysis of Fabricated Nanofibers, (F) Pore Size Distribution of PCI and PCI@GNS Nanofiber-Based Scaffolds, (G) Swelling Ratio of NFs, and (H) In Vitro Degradation Profile of Fabricated NFs. Note. FTIR: Fourier-transform infrared spectroscopy; PCI: Polycaprolactone; GNS: Gold nanostar; NF: Nanofibrous

NF-based scaffolds ranged from 2.3 N to 4 N, which is crucial for in vivo applications. Therefore, these scaffolds are more suitable for applications involving cancellous bone regeneration, as opposed to cortical bone, due to

their structural and mechanical properties. However, it should be noted that immersion in PBS significantly reduces the mechanical properties of the NFs (24). While the mechanical properties of NF scaffolds,

designed as biodegradable and temporary structures, significantly differ from those of dense, load-bearing permanent implants, it is critical for swollen scaffolds to exhibit adequate stiffness. This ensures proper surgical handling and facilitates secure placement of the graft during implantation (21). In comparison with PCL NFs, PCL-GNS NFs have low mechanical strength and elastic modulus. The presence of GNSs in the polymer structure leads to a notable reduction in mechanical stability in our experiments. The incorporation of GNSs into polymer scaffolds has been observed to reduce the mechanical strength of the resulting composites, likely due to the efficient transfer of mechanical stress facilitated by GNSs. Additionally, it has been reported that the presence of GNSs decreases the degree of mechanical interlocking both among NPs and between NPs and polymer chains, leading to the formation of weak points within the polymer matrix (25).

### Swelling Behavior

The water absorption capacity of tissue engineering scaffolds plays a critical role in determining the scaffold's ability to absorb biological fluids, facilitate nutrient diffusion, and enable the transport of metabolic waste products within the biomaterial matrix (26). The aforementioned attributes can be preserved by employing a high swelling ratio in the constructed scaffolds. All samples exhibited significant potential for swelling (Figure 4G) when it came to the absorption of water by dry scaffolds. Following prolonged soaking, the swelling ratio significantly rose, indicating a greater amount of water absorption. However, the rate of water absorption decreased, and the scaffold eventually reached a state of swelling equilibrium. The PCL@GNS scaffold illustrated the greatest rate of swelling in comparison to PCL scaffolds. Although the inclusion of GNSs affects the rate at which the samples swell (all samples swell after 1 hour), the swelling ratio decreases with an increase in reinforcement levels. The reduction in the swelling ratio with increasing GNS concentration is due to decreased scaffold porosity and a simultaneous decrease in polymer content within the structure. The swelling capacity of biopolymeric scaffolds is primarily governed by the interactions between polymer constituents and water molecules. Furthermore, these findings are consistent with previous reports concerning the swelling behavior of PCL-NF scaffolds (25,27).

### In Vitro Degradation

The degradative properties of scaffolds are critical for effective bone regeneration and are regarded as one of the most essential features for scaffolds intended for BTE. Ideally, the degradation rate of the scaffold should closely correspond to the rate of new tissue formation, thereby enabling seamless tissue regeneration. In the present study, the evaluation of the stability of NFs over 21 days revealed that approximately 50% of the scaffold mass

had degraded during this timeframe. Among the several types of tested scaffolds, the PCL scaffold exhibited the highest degradation percentage, while the PCL@GNS scaffold showed the lowest degradation percentage (Figure 4H). The results also showed that including GNSs in PCL scaffolds reduces their biodegradability, and this reduction is proportional to the increase in the percentage of GNSs. This phenomenon can be attributed to the low degradation rate of GNSs, which contributes to the overall stability of the scaffold during incubation (28, 29). However, recreating the surrounding environment in a laboratory setting after implanting the scaffold is extremely complicated since various types of proteases control the remodeling of the ECM. Therefore, the incorporation of GNSs may be advantageous for BTE applications, as their presence has the potential to inhibit the rapid degradation of scaffolds, thereby enhancing the longevity and structural integrity of implants during the tissue regeneration process (30).

### Hemocompatibility

The hemocompatibility of the scaffolds was assessed by evaluating the hemolysis generated by them. The findings suggested that the constructed scaffolds did not cause substantial hemolysis and can be regarded as structures that are compatible with blood (Figure 5A). The biological assessments further indicated that the constructed scaffolds were compatible with blood (showing minimal hemolysis) and compatible with cells. The NF with 10% GNSs resulted in the greatest cell growth. The findings indicate that artificial scaffolds can be used as scaffolds for BTE.

### Cell Viability

The potential clinical application of GNSs requires the confirmation of their biocompatibility and the absence of cytotoxic effects on normal cell lines. To assess this issue, the viability of ADSCs cultured in the presence of fabricated GNSs was evaluated using the MTT assay at 1 day, 3 days, and 5 days (Figure 5B). On day 1, a concentration of 1.5 mg/mL GNSs resulted in a marked reduction in cell viability. However, by days 3 and 5, none of the tested GNS concentrations exhibited significant cytotoxicity, and cell viability remained comparable to that of the control group. The cytotoxicity of GNSs is significantly influenced by the particle size and concentration. According to a study, GNSs with sizes between 30 nm and 300 nm do not have any noticeable harmful effects on HeLa cells (31). However, there is ongoing debate about the outcomes of GNS cytotoxicity, which may be attributed to differences in the synthesis technique of GNSs and the assays used to evaluate cytotoxicity (32). Composites must maintain inertness within the human body and exhibit compatibility with bone growth upon implantation. Furthermore, scaffolds must possess both biocompatibility and appropriate physicochemical properties. The results indicated that none of the scaffolds



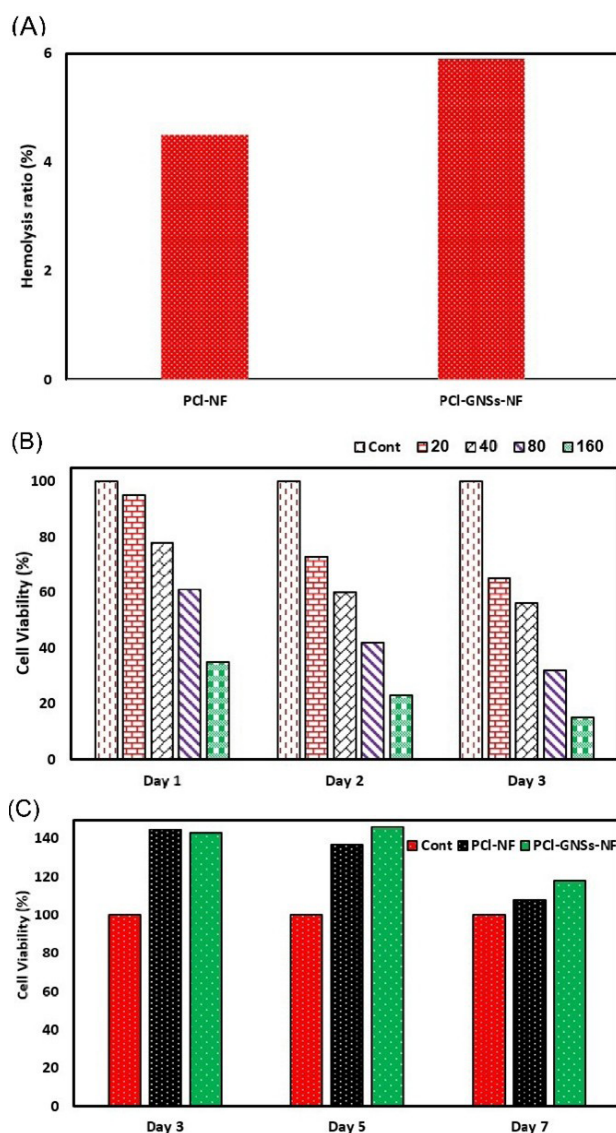


**Figure 5.** (A) Hemolysis Value of the PCI and PCI@GNS NF-Based Scaffold, (B) Cell Viability of ADSCs Cultured at Different Concentrations of GNSs for 1 Day, 3 Days, and 5 Days, and (C) Cell Viability Control, PCI, and PCI@GNS NF-Based Scaffolds for 3 Days, 5 Days, and 7 Days. Note. PCI: Polycaprolactone; NF: Nanofibrous; ADSC: Adipose-derived stem cells; GNS: Gold nanostar

exhibited cytotoxic effects when compared to the control group of two-dimensionally cultured cells over 3 days, 5 days, and 7 days, demonstrating comparable cell viability across all groups (Figure 5C). In addition, the PCI@GNSs demonstrated considerably greater cell viability than the control group at both the 3-day and 5-day time points. The biocompatibility qualities are significantly influenced by the composition of the scaffolds. The United States Food and Drug Administration has approved the utilization of PCL as a biomaterial. The cytotoxicity data obtained in this study confirmed the biocompatibility of the constituent polymers used in the scaffold fabrication (33).

## Conclusion

In this study, an NF scaffold was successfully developed by integrating GNSs into a polymeric matrix primarily composed of PCL. The GNSs were initially synthesized and

subsequently incorporated into the polymeric network to fabricate PCL-based nanocomposite scaffolds with varying concentrations of GNSs. Incorporating GNSs significantly influenced the resulting scaffolds' structural, mechanical, and biological properties. The fabricated NF scaffolds exhibited optimal swelling behavior, which is a critical parameter for supporting cellular activities and maintaining the structural integrity of scaffolds in biological environments. Furthermore, adding GNSs markedly enhanced the mechanical characteristics of the scaffolds, which are essential for applications in load-bearing regions. This improvement in mechanical properties was coupled with a slight reduction in porosity, a trade-off that could potentially contribute to improved scaffold stability without severely compromising its ability to support tissue ingrowth. An additional notable outcome of incorporating GNSs into the polymeric matrix was the observed extension in the hydrolytic degradation period of the scaffolds. This slower degradation profile suggests that the presence of GNSs can effectively delay the disintegration of the scaffold post-implantation, ensuring prolonged structural support during the critical stages of tissue regeneration. This characteristic is particularly beneficial for craniofacial bone regeneration, where sustained scaffold functionality is paramount to successful clinical outcomes. Biocompatibility studies conducted on ADSCs revealed that the constructed scaffolds demonstrated minimal cytotoxicity, confirming their suitability for biomedical applications. While a slight reduction in cell survival was observed compared to ADSCs cultivated on traditional two-dimensional substrates, this outcome was anticipated due to the inherent differences in cellular behavior between two-dimensional and three-dimensional systems. Importantly, the PCL@GNS NF scaffolds illustrated significantly higher cell viability compared to the control group when evaluated on the 3rd and 5th days of cultivation, further validating their potential as a favorable biomaterial for tissue engineering applications. In conclusion, the NF scaffolds developed in this study possessed the desired combination of mechanical strength, controlled degradation, cellular compatibility, and minimal cytotoxicity, making them highly suitable candidates for implantable biomaterials in the regeneration of craniofacial bone defects. These findings underscore the potential of GNS-reinforced polymeric scaffolds to address critical challenges in BTE and pave the way for future advancements in regenerative therapies.

## Acknowledgments

The authors of this article are grateful to Hamadan University of Medical Sciences for their financial support in conducting research.

## Authors' Contribution

**Conceptualization:** Alireza Koushki, Abolfazl Akbarzadah.

**Data curation:** Sonia Fathi-Karkan.

**Formal analysis:** Shayesteh Fathi.

**Funding acquisition:** Saber Ganji.

**Investigation:** Parisa Besharati.



**Methodology:** Negar Sedghi Aminabad.

**Project administration:** Maziar Malekzadeh Kebria.

**Resources:** Zahra Ebrahimvand Dibazar.

**Software:** Zahra Ebrahimvand Dibazar.

**Supervision:** Seyedeh Parvaneh Moosavi.

**Validation:** Sonia Fathi-Karkan.

**Visualization:** Saber Ganji and Shayesteh Fathi.

**Writing—original draft:** Alireza Koushki, Abolfazl Akbarzadah.

**Writing—review & editing:** Seyedeh Parvaneh Moosavi and Zahra Ebrahimvand Dibazar.

### Competing Interests

The authors declare that there is no potential conflict of interests in the present study.

### Data Availability Statement

The authors confirm that the data supporting the findings of this study are available within the article.

### Ethical Approval

The protocol of this in vitro study was approved by the Ethics Committee of Mashhad University of Medical Sciences.

### Funding

The study was supported by a grant from the Vice-Chancellor for Research at Mashhad University of Medical Sciences.

### References

1. Zhu G, Zhang T, Chen M, Yao K, Huang X, Zhang B, et al. Bone physiological microenvironment and healing mechanism: basis for future bone-tissue engineering scaffolds. *Bioact Mater.* 2021;6(11):4110-40. doi: [10.1016/j.bioactmat.2021.03.043](https://doi.org/10.1016/j.bioactmat.2021.03.043).
2. Nekounam H, Kandi MR, Shaterabadi D, Samadian H, Mahmoodi N, Hasanzadeh E, et al. Silica nanoparticles-incorporated carbon nanofibers as bioactive biomaterial for bone tissue engineering. *Diam Relat Mater.* 2021;115:108320. doi: [10.1016/j.diamond.2021.108320](https://doi.org/10.1016/j.diamond.2021.108320).
3. Li Q, Ge L, Wan W, Jiang J, Zhong W, Ouyang J, et al. Magnetically guided fabrication of multilayered iron oxide/polycaprolactone/gelatin nanofibrous structures for tissue engineering and theranostic application. *Tissue Eng Part C Methods.* 2015;21(10):1015-24. doi: [10.1089/ten.TEC.2015.0051](https://doi.org/10.1089/ten.TEC.2015.0051).
4. Liu T, Xu J, Pan X, Ding Z, Xie H, Wang X, et al. Advances of adipose-derived mesenchymal stem cells-based biomaterial scaffolds for oral and maxillofacial tissue engineering. *Bioact Mater.* 2021;6(8):2467-78. doi: [10.1016/j.bioactmat.2021.01.015](https://doi.org/10.1016/j.bioactmat.2021.01.015).
5. Shuai C, Yang W, He C, Peng S, Gao C, Yang Y, et al. A magnetic micro-environment in scaffolds for stimulating bone regeneration. *Mater Des.* 2020;185:108275. doi: [10.1016/j.matdes.2019.108275](https://doi.org/10.1016/j.matdes.2019.108275).
6. Woo KM, Chen VJ, Ma PX. Nano-fibrous scaffolding architecture selectively enhances protein adsorption contributing to cell attachment. *J Biomed Mater Res A.* 2003;67(2):531-7. doi: [10.1002/jbm.a.10098](https://doi.org/10.1002/jbm.a.10098).
7. Siddiqui N, Asawa S, Birru B, Baadhe R, Rao S. PCL-based composite scaffold matrices for tissue engineering applications. *Mol Biotechnol.* 2018;60(7):506-32. doi: [10.1007/s12033-018-0084-5](https://doi.org/10.1007/s12033-018-0084-5).
8. Ragaert K, Van de Velde S, Cardon L, de Somer F. Methods for improved flexural mechanical properties of 3D-plotted PCL-based scaffolds for heart valve tissue engineering. 5th International conference on Polymers and Moulds Innovations (PMI 2012); 2012.
9. Vial S, Reis RL, Oliveira JM. Recent advances using gold nanoparticles as a promising multimodal tool for tissue engineering and regenerative medicine. *Curr Opin Solid State Mater Sci.* 2017;21(2):92-112. doi: [10.1016/j.cossms.2016.03.006](https://doi.org/10.1016/j.cossms.2016.03.006).
10. Zhou S, Pan Y, Zhang J, Li Y, Neumann F, Schwerdtle T, et al. Dendritic polyglycerol-conjugated gold nanostars with different densities of functional groups to regulate osteogenesis in human mesenchymal stem cells. *Nanoscale.* 2020;12(47):24006-19. doi: [10.1039/d0nr06570f](https://doi.org/10.1039/d0nr06570f).
11. Vinnacombe-Willson GA, García-Astrain C, Troncoso-Afonso L, Wagner M, Langer J, González-Callejo P, et al. Growing gold nanostars on 3D hydrogel surfaces. *Chem Mater.* 2024;36(10):5192-203. doi: [10.1021/acs.chemmater.4c00564](https://doi.org/10.1021/acs.chemmater.4c00564).
12. Yi DK, Nanda SS, Kim K, Tamil Selvan S. Recent progress in nanotechnology for stem cell differentiation, labeling, tracking and therapy. *J Mater Chem B.* 2017;5(48):9429-51. doi: [10.1039/c7tb02532g](https://doi.org/10.1039/c7tb02532g).
13. Gupta A, Singh S. Multimodal potentials of gold nanoparticles for bone tissue engineering and regenerative medicine: avenues and prospects. *Small.* 2022;18(29):e2201462. doi: [10.1002/sml.202201462](https://doi.org/10.1002/sml.202201462).
14. Shan H, Zhou X, Tian B, Zhou C, Gao X, Bai C, et al. Gold nanorods modified by endogenous protein with light-irradiation enhance bone repair via multiple osteogenic signal pathways. *Biomaterials.* 2022;284:121482. doi: [10.1016/j.biomaterials.2022.121482](https://doi.org/10.1016/j.biomaterials.2022.121482).
15. Filipowska J, Tomaszewski KA, Niedźwiedzki Ł, Walocha JA, Niedźwiedzki T. The role of vasculature in bone development, regeneration and proper systemic functioning. *Angiogenesis.* 2017;20(3):291-302. doi: [10.1007/s10456-017-9541-1](https://doi.org/10.1007/s10456-017-9541-1).
16. Xia Y, Sun J, Zhao L, Zhang F, Liang XJ, Guo Y, et al. Magnetic field and nano-scaffolds with stem cells to enhance bone regeneration. *Biomaterials.* 2018;183:151-70. doi: [10.1016/j.biomaterials.2018.08.040](https://doi.org/10.1016/j.biomaterials.2018.08.040).
17. Qiao M, Tang W, Xu Z, Wu X, Huang W, Zhu Z, et al. Gold nanoparticles: promising biomaterials for osteogenic/adipogenic regulation in bone repair. *J Mater Chem B.* 2023;11(11):2307-33. doi: [10.1039/d2tb02563a](https://doi.org/10.1039/d2tb02563a).
18. Azizi M, Pakravan A, Valizadeh H, Rahbarghazi R, Dianat-Moghadam H, Bani F, et al. Fabrication and characterization smart gold-polymer nanostructure as promising theranostic agent for dual-imaging and chemo-photothermal therapy of cancer: an in vitro study. *J Photochem Photobiol A Chem.* 2024;450:115459. doi: [10.1016/j.jphotochem.2024.115459](https://doi.org/10.1016/j.jphotochem.2024.115459).
19. Liu Y, Ashton JR, Moding EJ, Yuan H, Register JK, Fales AM, et al. A plasmonic gold nanostar theranostic probe for in vivo tumor imaging and photothermal therapy. *Theranostics.* 2015;5(9):946-60. doi: [10.7150/thno.11974](https://doi.org/10.7150/thno.11974).
20. Acosta Santamaría VA, García Aznar JM, Ochoa I, Doblare M. Effect of sample pre-contact on the experimental evaluation of cartilage mechanical properties. *Exp Mech.* 2013;53(6):911-7. doi: [10.1007/s11340-012-9698-x](https://doi.org/10.1007/s11340-012-9698-x).
21. Echave MC, Erezuma I, Golafshan N, Castilho M, Kadumudi FB, Pimenta-Lopes C, et al. Bioinspired gelatin/bioceramic composites loaded with bone morphogenetic protein-2 (BMP-2) promote osteoporotic bone repair. *Biomater Adv.* 2022;134:112539. doi: [10.1016/j.msec.2021.112539](https://doi.org/10.1016/j.msec.2021.112539).
22. Kumar R, Siril PF. Enhancing the solubility of fenofibrate by nanocrystal formation and encapsulation. *AAPS PharmSciTech.* 2018;19(1):284-92. doi: [10.1208/s12249-017-0840-z](https://doi.org/10.1208/s12249-017-0840-z).
23. Mouro C, Gomes AP, Ahonen M, Fangueiro R, Gouveia IC. *Chelidonium majus* L. incorporated emulsion electrospun PCL/PVA-PEC nanofibrous meshes for antibacterial wound dressing applications. *Nanomaterials (Basel).* 2021;11(7):1785. doi: [10.3390/nano11071785](https://doi.org/10.3390/nano11071785).
24. Wu L, Zhang J, Jing D, Ding J. "Wet-state" mechanical properties of three-dimensional polyester porous scaffolds.

- J Biomed Mater Res A. 2006;76(2):264-71. doi: [10.1002/jbm.a.30544](https://doi.org/10.1002/jbm.a.30544).
25. Samadian H, Khastar H, Ehterami A, Salehi M. Bioengineered 3D nanocomposite based on gold nanoparticles and gelatin nanofibers for bone regeneration: in vitro and in vivo study. *Sci Rep*. 2021;11(1):13877. doi: [10.1038/s41598-021-93367-6](https://doi.org/10.1038/s41598-021-93367-6).
  26. Liu M, Dai L, Shi H, Xiong S, Zhou C. In vitro evaluation of alginate/halloysite nanotube composite scaffolds for tissue engineering. *Mater Sci Eng C Mater Biol Appl*. 2015;49:700-12. doi: [10.1016/j.msec.2015.01.037](https://doi.org/10.1016/j.msec.2015.01.037).
  27. Zhu J, Jiang G, Song G, Liu T, Cao C, Yang Y, et al. Incorporation of ZnO/bioactive glass nanoparticles into alginate/chitosan composite hydrogels for wound closure. *ACS Appl Bio Mater*. 2019;2(11):5042-52. doi: [10.1021/acsabm.9b00727](https://doi.org/10.1021/acsabm.9b00727).
  28. Guo X, Shi H, Zhong W, Xiao H, Liu X, Yu T, et al. Tuning biodegradability and biocompatibility of mesoporous silica nanoparticles by doping strontium. *Ceram Int*. 2020;46(8, Part B):11762-9. doi: [10.1016/j.ceramint.2020.01.210](https://doi.org/10.1016/j.ceramint.2020.01.210).
  29. Cheheltani R, Ezzibdeh RM, Chhour P, Pulaparthi K, Kim J, Jurcova M, et al. Tunable, biodegradable gold nanoparticles as contrast agents for computed tomography and photoacoustic imaging. *Biomaterials*. 2016;102:87-97. doi: [10.1016/j.biomaterials.2016.06.015](https://doi.org/10.1016/j.biomaterials.2016.06.015).
  30. Kus-Liśkiewicz M, Fickers P, Ben Tahar I. Biocompatibility and cytotoxicity of gold nanoparticles: recent advances in methodologies and regulations. *Int J Mol Sci*. 2021;22(20):10952. doi: [10.3390/ijms222010952](https://doi.org/10.3390/ijms222010952).
  31. Khlebtsov N, Dykman L. Biodistribution and toxicity of engineered gold nanoparticles: a review of in vitro and in vivo studies. *Chem Soc Rev*. 2011;40(3):1647-71. doi: [10.1039/c0cs00018c](https://doi.org/10.1039/c0cs00018c).
  32. Mahto SK, Charwat V, Ertl P, Rothen-Rutishauser B, Rhee SW, Sznitman J. Microfluidic platforms for advanced risk assessments of nanomaterials. *Nanotoxicology*. 2015;9(3):381-95. doi: [10.3109/17435390.2014.940402](https://doi.org/10.3109/17435390.2014.940402).
  33. Bernard M, Jubeli E, Pungente MD, Yagoubi N. Biocompatibility of polymer-based biomaterials and medical devices - regulations, in vitro screening and risk-management. *Biomater Sci*. 2018;6(8):2025-53. doi: [10.1039/c8bm00518d](https://doi.org/10.1039/c8bm00518d).